Article | Received 29 January 2025; Accepted 22 April 2025; Published 6 May 2025
https://doi.org/10.55092/sc20250010

Effects of environmental factors on robotic building processes: a physical experimental investigation

Cheav Por Chea[1,*], Yu Bai[1,*], Yihai Fang[1] and Elahe Abdi[2]

[1] Department of Civil Engineering, Monash University, Clayton, VIC 3800, Australia
[2] Department of Mechanical and Aerospace Engineering, Monash University, Clayton, VIC 3800, Australia

* Correspondence author(s); E-mail(s): paul.chea@monash.edu; yu.bai@monash.edu.

Highlights:

- Effects of luminance on robotic assembly accuracy quantified via physical experiments.
- Building succeeded by robotic system with AprilTag under low-light conditions.
- Obstacle patterns significantly impact mobile robot orientation and assembly success.
- Experimental data provided to improve robotic construction for site conditions.

Abstract: As robotic applications in building processes increase, the majority of studies focus on development of algorithms for object targeting, path planning, and localisation. Very limited attention is given to environmental factors, such as varying luminance and presence of undetected obstacles, that are common on construction sites and can significantly influence the robotic system performance. To address the gap, this work investigates the effects of environmental conditions on robot performance in structural assembly. A series of physical experiments was conducted in a laboratory setting to evaluate the effects of different lighting conditions on the positional accuracy of the robotic arm, the time required to install components, and the overall successful rate of the robotic assembly. The coordinates and orientations of installed AprilTag markers, captured by a red green blue-depth (RGB-D) camera, were then analysed to determine the effects of luminance levels on the accuracy of the positioning robotic system in two different assembly tasks. Furthermore, under constant luminance conditions, obstacles were arranged in various patterns along the path of a mobile robot to evaluate changes in trajectory and alignment disturbances. Differences in robot orientation, installation times, and completion status of the assembly tasks were also recorded to understand the impact of obstacle configurations on the efficiency and adaptability of the robotic system in structural assembly.

Keywords: robotic arm; mobile robot; luminance; obstacle; building process

1. Introduction

Robotic technologies have been increasingly considered in construction industry, particularly for tasks such as concrete 3D printing, surveying, bricklaying, and more recently structural assembly. In assembly processes, robotic technologies have largely been applied to the installation of non-structural components, which do not directly contribute to load-bearing capacity and are usually installed after the main structure is formed. For example, a robotic system was developed for installation of glass façades using a vacuum end-effector and a mobile platform [1], though human assistance was required to adjust the installation position of the façade. In another study, a humanoid robot was employed to install plasterboard [2]. In case of the assembly of load-bearing structures such as frames, the accuracy requirements are much higher, and often cooperation of multiple robots is needed. For instance, in order to assemble a steel frame, bolting robots [3] and an elevation lifting system [4,5] were developed and integrated into a platform to enable communication and enhance precision [6].

From the literature review, it can be seen that existing studies mainly focus on the installation of non-structural components (e.g. façades or wall panels) or on specific tasks in the assembly process of a load-bearing structure (e.g. bolting or frame elevation). In a previous study [7], a multi-robot system was developed to automatically assemble a load-carrying glass fibre reinforced polymer (GFRP) reciprocal frame (RF) structure with a span of 4.5 m, using two teams of robots (each team included a robotic arm and a mobile robot). The RF structure was introduced to reduce the complexity of structural connections [8], and temporary magnetic connections were innovatively proposed to mitigate the positional inaccuracy of the robotic system. This construction robotic process included positioning (component targeting), adjusting (robot alignment), and fixing (component installation), as also suggested in the literature [9]. Key parameters, such as the effective magnetic coupling range, the positional accuracy of the robotic arms, and the offset of the mobile robot over a one-metre travel distance, were then investigated [10].

In actual building environments, dynamic and unpredictable conditions may be present, such as variable luminance, obstacles, and ongoing human activities. These factors may have unexpected impacts on the efficiency and accuracy of robotic operations. To assess the performance and adaptability of robots in real-world settings, previous investigations were conducted through deployment of robots in various environments, such as studies on the influence of weather on autonomous vehicles [11–13], the effect of lighting on terrain recognition for outdoor robots [14,15], and the performance of robotic tower cranes in diverse settings (e.g. indoor, outdoor, and active construction sites) [16,17]. Portable robots equipped with ultra-wideband (UWB) and light detection and ranging (LiDAR) technologies were employed to operate in dense fog conditions with improved performance [18,19]. Although direct evaluations of the performance of robots in real-world environments can provide valuable insights, environmental parameters, such as luminance and obstacle distribution, are difficult to consistently replicate, adjust, or separate from other factors (e.g. dust, wind, temperature). Laboratory experiments, on the other hand, can offer a controlled environment where key environmental factors, such as luminance and obstacle distribution, can be adjusted to achieve consistent and repeatable conditions.

On a physical site, lighting conditions (*i.e.* luminance) are likely to affect the success of robotic structural assembly since the image-based positioning algorithm in the robotic system may misrecognise or may not be able to detect the images in poor light environments [20–22]. Existing studies have shown

that luminance levels influence the accuracy of shape-based methods to categorise bolt sizes [23] and determine their spatial positions [24]. Other image-based tasks, such as detecting safety helmets [25] or identifying defects in metro tunnel surfaces [26], are also affected by illumination. It is true that challenges are faced for robotic construction in unstable environments and there are clear limitations of current technologies [27, 28]. To address positional inaccuracy caused by luminance variation, a multi-sensor robotic system was developed in a previous study [29], incorporating an inertial measurement unit (IMU), infrared sensor, RGB camera, and LiDAR for localisation and mapping. Under favourable lighting conditions (e.g., 17,490 lx), this system achieved an average positional inaccuracy of about 12 mm, which was superior to other systems reporting errors between 15 mm and 20 mm. However, when the luminance dropped to 22 lx, the accuracy of the robotic system declined, with positional inaccuracy increasing to 18 mm. This highlights that, even with the integration of multiple sensors, lighting conditions remain a critical factor influencing system performance. While a positional inaccuracy of 18 mm may be acceptable for localisation or mapping, it is insufficient for high-precision tasks such as robotic assembly, where the tolerance can be as low as 2 mm [30]. To meet this requirement, fiducial marker systems such as the AprilTag have been employed in the robotic system [7], offering high-precision position and orientation data using only an RGB-D camera and markers. However, the performance of such robotic system under varying lighting conditions remains underexplored. Furthermore, objects or obstacles on site may physically impede robots from moving forward or detour them from their trajectories. To avoid these obstacles, various algorithms for global path planning, such as graph search methods, sampling-based methods, evolutionary computation methods, artificial intelligence, and local path planning approaches such as the dynamic window approach (DWA) were implemented [31]. However, unstructured terrains or undetected objects on site may cause mobile robots to slip, sending the associated robotic arms off trajectory or blocking the robots from moving forward [32–34]. It also can be seen that there is very limited research on quantification and understanding on the impact of environmental factors such as luminance and undetected obstacles on robotic systems.

In this study, the effects of environmental luminance and obstacle patterns on a multi-robot system proposed in a previous study [7] were investigated. Firstly, the luminosities on the surfaces of AprilTag markers used to position the components were measured under different luminance scenarios, ranging from bright to moderate light and relatively dark conditions. Accordingly, the coordinates and orientation of the markers were observed through the red green blue-depth (RGB-D) camera. Such measurements can be used to understand the effect of the luminance on the accuracy of the positioning system. In addition, two assembly tasks were conducted to investigate the construction time and the success rate of the installation in various luminance scenarios. In well-conditioned indoor light, humps were arranged in different patterns on the path of the mobile robot to examine potential changes in its trajectory and disturbances in its alignment. The difference in the orientation of the mobile robot when passing the humps, the construction time and the completion status of structural assembly were also investigated under the variation of obstacle patterns. This study aims to experimentally investigate the variations in positioning inaccuracy, construction efficiency, and success rate under different lighting and obstacle conditions. Therefore, valuable data from physical experimental investigations, as currently very limited in literature, can be received to inform improvements to robotic systems and to support the design for robotic construction.

2. Experimental setup and procedure

The assembly of reciprocal frame structures was automated by a multi-robot system in the previous study [7]. The multi-robot system was developed with two teams, each comprising a robotic arm (e.g. UR10e) equipped with grippers (RG6) and an RGB-D camera (D435i) and a mobile robot (e.g. MiR100), to assemble components of a reciprocal frame (RF) structure. Similar structural form and robotic system were used in this study to examine the effects of typical environmental factors on the assembly process. RF structures comprised of two types of components (*i.e.* main components and cross components), where the main components are members that form the primary load-bearing framework, while the cross components are positioned transversely to transfer loads to the main components. To ensure a better identification, the main components are labelled as either MC-*i*a or MC-*i*b based on their location on two sides of the reciprocal structure (see Figure 1), and the cross components are labelled as CC-*i*. To reduce duration of each test, instead of installation of all the components for the RF structures as demonstrated in the previous study [7], only the installations of components MC-2a and CC-3 (*i.e.* one main component and one cross component) were employed for the investigation of the effects from environmental parameters (*i.e.* luminance and obstacle pattern). The structural components were made of pultruded glass fibre reinforced polymer (GFRP) with a circular hollow section (CHS) of an outer/inner diameter of 31/28 mm. The length of each main component (*i.e.* MC-1a, MC-1b, MC-2a and MC-2b) was 1.5 m, and the length of each cross component (*i.e.* CC-1, CC-2 and CC-3) was 1 m.

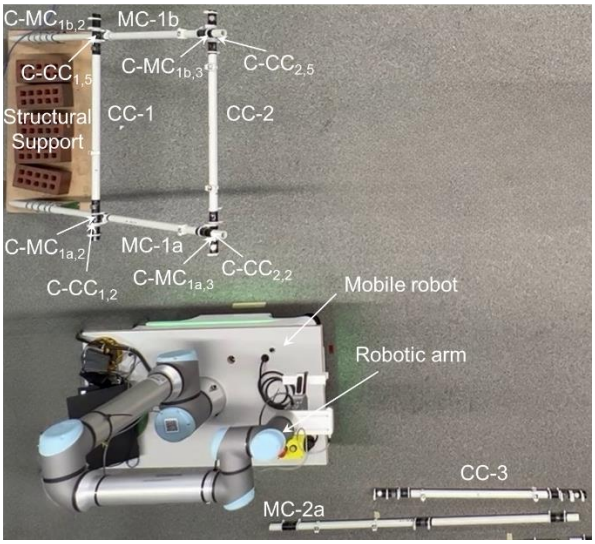

Figure 1. Experimental setup with MC-2a and CC-3 in storage area prior to their installations.

To prepare for the experiments, as shown in Figure 1, components MC-1a and MC-1b were first attached to the structural support, and then CC-1 was placed on the components MC-1a and MC-1b, with the magnets C-$CC_{1,2}$ and C-$CC_{1,5}$ of component CC-1 matched to the magnets C-$MC_{1a,2}$ of the components MC-1a and C-$MC_{1b,2}$ of the components MC-1b on both sides of the RF structure. Similarly, CC-2 was also placed on components MC-1a and MC-1b with the magnets C-$CC_{2,2}$ and C-$CC_{2,5}$ of component CC-2 matched with magnets C-$MC_{1a,3}$ of MC-1a and magnets C-$MC_{1b,3}$ of MC-1b on both sides of the structure. Meanwhile, components MC-2a and CC-3 were placed on the storage area to be ready for their installations.

In this way, the installations of components MC-2a and CC-3 (*i.e.* one main component and one cross component) were employed for the investigation of the effects from environmental parameters (*i.e.* luminance and obstacle pattern). In total, three cross components (*i.e.* CC-1, CC-2, CC-3), four main components (*i.e.* MC-1a, MC-1b, MC-2a and MC-2b), and a structural support were involved in the experiments; while components CC-1, CC-2, MC-1a and MC-1b were already in their positions prior to the installations of MC-2a and CC-3 (see Figure 1). Figure 2 illustrated the locations of the mobile robot to install MC-2a and CC-3, as well as the locations of the components (*i.e.* CC-1, CC-2, CC-3, MC-1a and MC-2a) during the construction.

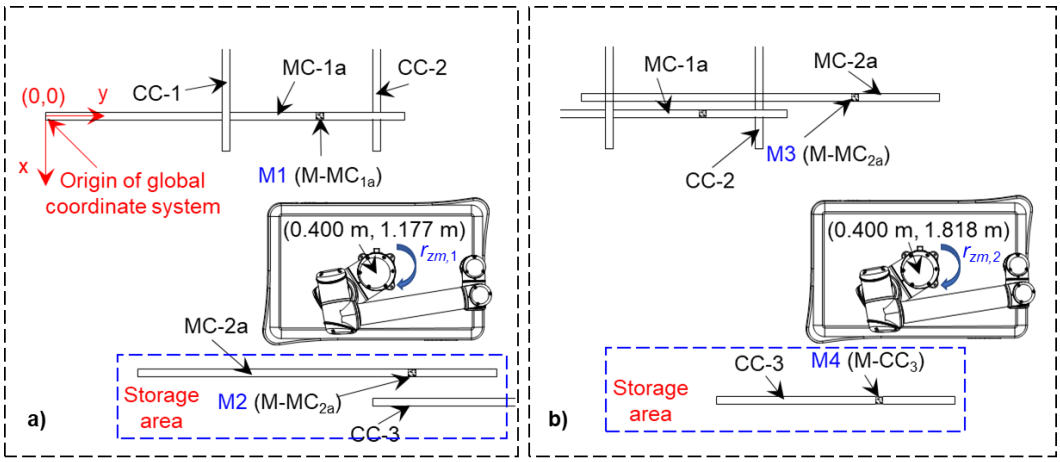

Figure 2. Installation process of **(a)** main component MC-2a and **(b)** cross component CC-3, with locations of fiducial markers M-MC_{1a}, M-MC_{2a} from MC-2a in the storage area and from installed component MC-2a, M-CC_3 (*i.e.* M1, M2, M3 and M4).

2.1. Environmental luminance investigation

Different locations of the markers (*i.e.* M-MC_{1a}, M-MC_{2a}, and M-CC_3) were considered to study the effect of environmental luminance on the determination of coordinates and orientations of the markers in these locations. As shown in Figure 2, the locations of markers M-MC_{1a}, M-MC_{2a}, and M-CC_3 during the installation process of components MC-2a and CC-3 were coded as M1, M2, M3 and M4. Specifically, M1 corresponded to the location of marker M-MC_{1a} on the installed main component MC-1a, and was used to align the mobile robot for the installation of component MC-2a; M2 corresponded to the location of marker M-MC_{2a} on the main component MC-2a which was placed on the storage area, and was used to allow the robotic arm to target component MC-2a; M3 corresponded to the location of marker M-MC_{2a} on the installed MC-2a, and was used for the alignment of the mobile robot to install component CC-3; and M4 corresponded to the location of the marker M-CC_3 on the CC-3 which was placed on the storage area, and was for robotic arm to target component CC-3.

Lighting condition (*i.e.* luminance) of the experimental environment was achieved by two batten lights (*i.e.* batten lights N and S as shown in Figure 3) installed on the ceiling of the laboratory, where batten light S was above the robots (*i.e.* the mobile robot and robotic arm) and batten light N was away from the robots as shown in Figure 3. The experimental program consisted of four scenarios described below:

Scenario L1: both batten lights N and S were turned on as shown in Figure 3(a). The environmental luminance in this scenario was the brightest compared to those in the other scenarios and this corresponded to a well-conditioned indoor environmental luminance.

Scenario L2: batten light S was on and batten light N was off as shown in Figure 3(b). This corresponded to the indoor low lighting environment.

Scenario L3: batten light N was on and light S was off as shown in Figure 3(c). The brightness of the storage area aside of robots in this scenario was darker than that in scenario L2, since the batten light N was far from the robots.

Scenario L4: both batten lights S and N were turned off as shown in Figure 3(d). This scenario was used to simulate a poor lighting environment.

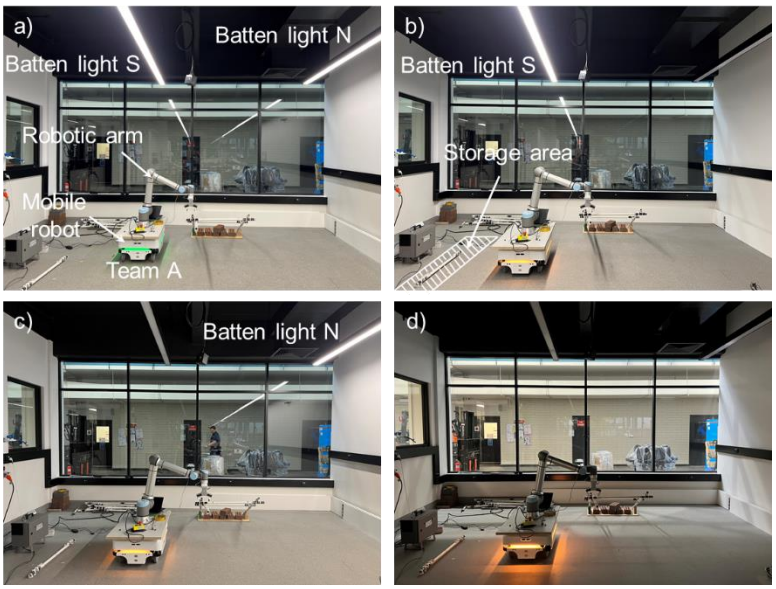

Figure 3. Laboratory environment with batten lights to simulate different luminance conditions; **(a)** L1 (both batten lights N and S on); **(b)** L2 (batten light S on and light N off); **(c)** L3 (batten light N on and light S off); **(d)** L4 (both batten lights off).

The coordinates and orientation of the markers (*i.e.* M1, M2, M3 and M4) observed through the positioning system (*i.e.* AprilTag) were studied in different environmental luminance (*i.e.* L1, L2, L3 and L4). This was conducted by subscribing the coordinates $(x_{i,j}, y_{i,j})_{cam}$ and orientation $(r_{zi,j})_{cam}$ in the camera coordinate system (see Figure 4) of the marker (at M1, M2, M3 or M4 as shown in Figure 2) using the camera attached on the end-effector of the robotic arm. Subscript i represents the marker location and j indicates the environmental luminance. For example, $x_{1,3}$ means the coordinate of the marker at M1 in x_c axis of the camera coordinate system, achieved from environmental luminance L3. The subscription was done after the mobile robot was aligned parallel to component MC-1a for the marker at M1, or parallel to component MC-2a, for the marker at M3 through the AprilTag system using an RGB-D camera; or after aiming component MC-2a for the marker at M2 or component CC-3 for the marker at M4.

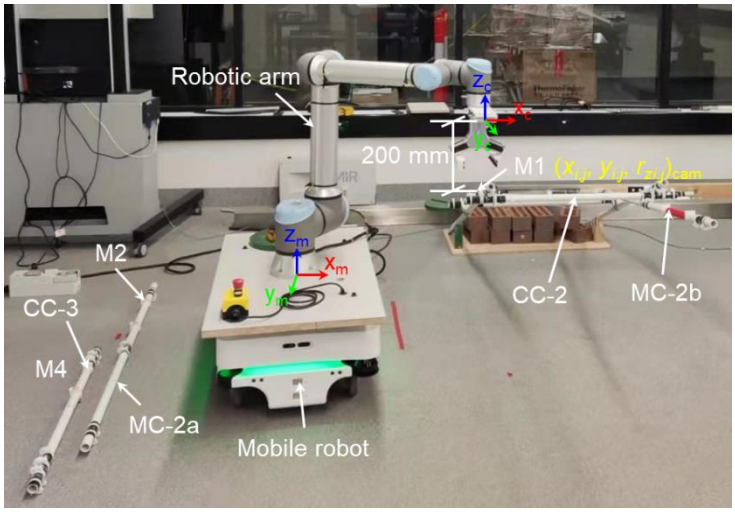

Figure 4. Experimental setup to investigate coordinates $(x_{i,j}, y_{i,j})_{cam}$ and orientation $(r_{zi,j})_{cam}$ of markers at M1, M2, M3 and M4 through positioning system in various luminance scenarios.

During the subscription, the relative positions and orientations between the camera and the markers at M1, M2, M3 or M4 remained constant in various environmental luminance (*i.e.* L1, L2, L3 and L4), subjected to the observation distance between the camera to the marker of 200 mm (as shown in Figure 4). In the experiments, the coordinates $(x_{i,j}\ y_{i,j})_{cam}$ and orientation $(r_{zi,j})_{cam}$ in camera coordinate system of each marker in each environmental luminance scenario were gathered every five seconds and for thirty times. During each test, the luminosities on the surface of the fiducial markers at four different locations of the construction site (*i.e.* M1, M2, M3, and M4 as shown in Figure 2) were measured using an illuminance meter (Yokogawa 510 01) and recorded accordingly. The illuminance meter can detect a wide range of luminance from 0.0 to 999 × 10^3 lx on a surface, and the tolerance of illuminance meter shall be about ± 4% if the luminance is lower than 3000 lx [35].

Furthermore, in order to investigate the effects of the environmental luminance on the efficiency and completion of the installation of MC-2a and CC-3, an experiment started with the mobile robot moving to the location (0.400 m, 1.177 m) in the global coordinate system as shown in Figure 2, to install the component MC-2a, where the origin of the system was at the structural support as shown in Figure 2(a). The mobile robot would then align parallel to the installed component MC-1a through marker M-MC_{1a} at M1 using AprilTag fiducial marker system. Subsequently, the robotic arm would target the component MC-2a in the storage area (see Figure 2(a)) through marker M-MC_{2a} at M2 and install component MC-2a following the frameworks outlined in the previous study [7]. Meanwhile, the component MC-2b on the other side of the structure, which was supposed to be installed by another robot, was assembled manually in this case to focus on the effects of luminance and obstacle disturbance on the installations of the targeted components. After the components MC-2a and MC-2b were installed, the mobile robot would move to the next location (*i.e.* 0.400 m, 1.818 m in the global coordinate system, see Figure 2(b)) to install component CC-3. Then, the mobile robot would again align parallel to MC-2a according to the marker M-MC_{2a} at M3 and component CC-3 would be targeted from the storage area according to the marker M-CC_3 at M4. In this way, component CC-3 could be then grabbed and moved to the installed position.

Thirteen experiments (*i.e.* installations of MC-2a and CC-3) were conducted in each scenario to investigate the effects of environmental luminance on the construction time and completion status of the robotic system. During the experiments, time to complete the installation was recorded in the main script of the robotic programme, corresponding to the duration from the time when the mobile robot arrived at the location (0.400 m, 1.177 m) for installing MC-2a to the time when CC-3 was installed (if proceeded that far). The standard deviation (σ) of this direction in an experimental scenario was then calculated using Equation (1).

$$\sigma = \sqrt[2]{\frac{\sum(T_i - \overline{T})^2}{N}} \quad (1)$$

where T_i is the duration of experiment i; N is the total number of experiments where the installations of MC-2a and CC-3 were completed; $\overline{T}$ is the average value of the experimental durations (only those of successful installations of MC-2a and CC-3 were considered). The completion status (failed or successful) and failure modes in this experimental scenario were also recorded and captured in different environmental luminance.

2.2. Obstacle disturbance investigation

In order to study the effects of obstacle patterns on the robotic structural assembly, the experimental scenarios were proceeded in the laboratory environment (with the luminance condition L1) using the mobile robot MiR100. This mobile robot has a weight capacity of 100 kg and is equipped with four corner caster wheels with a diameter of 125 mm and two middle drive wheels with a diameter of 125 mm [36]. The light detection and ranging (LiDAR) system of the mobile robot has a limitation that it cannot detect objects lower than 180 mm. Therefore, there is a risk that the mobile robot may collide with such low-lying obstacles. Humps, made of plywood with a height of 15 mm, width of 50 mm, and length of 250 mm, were placed on the ground at different distances from each other to form different obstacle patterns on the construction site as shown in Figure 5. It was noted that humps A and B were expected to change the direction of the mobile robot when it was passing over as the mobile robot was not able to detect such low-lying obstacles, while humps C and D were expected to interrupt the mobile robot when it was in alignment parallel to the installed component. As illustrated in Figure 5, L is the distance from the front wheels of the mobile robot to the humps A and/or B; D is the spacing between rows of humps A (or B) and C (or D). Five experimental scenarios were considered as follows, and thirteen tests were conducted in each scenario:

Scenario T1: only humps A and B were placed with a distance L of 400 mm from the front wheels of the mobile robot as shown in Figure 5(b).

Scenario T2: only hump A was placed with a distance L of 400 mm from the mobile robot as shown in Figure 5(c).

Scenario T3: humps A and B were placed with a distance L of 400 mm from the mobile robot, and humps C and D were placed with a spacing D of 150 mm from a and b as shown in Figure 5(d).

Scenario T4: only hump A was placed with a distance L of 400 from the mobile robot while humps C and D were placed with a distance D of 150 mm from a as shown in Figure 5(e).

Scenario T5: humps A and B were placed with a distance L of 400 mm from the mobile robot. Humps C and D were placed with a distance D of 100 mm from humps A and B as shown in Figure 5(f).

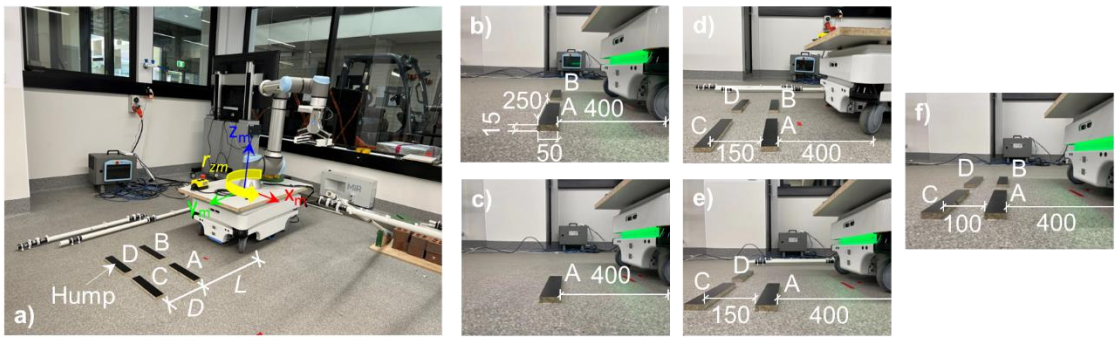

Figure 5. Experimental investigation on obstacle pattern effects: **(a)** overall setup; **(b)** scenario T1 (*L* of 400 mm) for humps A and B; **(c)** T2 (*L* of 400 mm for hump A only); **(d)** T3 (*L* of 400 mm for humps A and B) and (*D* of 150 mm for humps C and D); **(e)** T4 (*L* of 400 mm for hump A, *D* of 150 mm for humps C and D); **(f)** T5 (*L* of 400 mm for humps A and B, *D* of 100 mm for humps C and D) (unit: mm).

To study the effects of the obstacle patterns (*i.e.* T1, T2, T3 and L4) on the orientation of the mobile robot, efficiency, and successful rate of the installation of MC-2a and CC-3, the experiments proceeded with a similar experimental program used to investigate the effect of environmental luminance in Section 2.1. Specifically, the mobile robot moved to the location (0.400 m, 1.177 m, see Figure 2) and aligned to parallel with MC-1a. Then the robotic arm moved to the storage area to target and install MC-2a. Subsequently, the mobile robot passed humps A and B to the location (0.400 m, 1.818 m as shown Figure 2(b)) and aligned itself parallel to MC-2a. Then, CC-3 at the storage area was targeted and installed by the robotic arm.

During the experiments, the orientations of the mobile robot before and after (*i.e.* $r_{zm,1}$, $r_{zm,2}$ as shown in Figure 2) passing humps A and B or hump A only were recorded, and their difference (*i.e.* $\Delta r_{zm} = r_{zm,2} - r_{zm,1}$) were determined to study the effect of such obstacles on the orientation of the mobile robot, where $r_{zm,1}$ was achieved from subscribing marker M-MC$_{1a}$ at M1 after the robot was aligned parallel to MC-1a, *i.e.* $r_{zm,1} = (r_{z1,1})_{cam}$; $r_{zm,2}$ was achieved from subscribing marker M-MC$_{2a}$ at M3, *i.e.* $r_{zm,1} = (r_{z3,1})_{cam}$, after passing the humps and before proceeding alignment. The duration of the installation was also recorded in the main script of the robotic programme to investigate the effect of obstacle disturbance on the installation of components MC-2a and CC-3. In addition, the failure modes of the installation were also captured for further analysis. The battery of the mobile robot was charged to no less than 50% of its capacity (greater than 19.8 Ah) in order to remove the cases that the mobile robot in low power may not be able to pass the obstacles because of the reduction of output voltage (less than 24V).

3. Results and discussion

3.1. Environmental luminance effects

Figure 6 shows the luminosities of the markers at different locations (M1, M2, M3, and M4, see Figure 2) in various luminance scenarios (L1, L2, L3 and L4). As shown in Figure 6, for scenario L1 where both batten lights were on, the average luminance of M1 or M3 (*i.e.* 157 lx or 162 lx) located at the installed components (*i.e.* MC-1a or MC-2a) was about 35 lx brighter than those located at M2 or M4 (*i.e.* 124 lx or 121 lx), since the batten light N was far from the storage area and the luminosities of M2 and M4 in the storage area

were reduced by the shadow of the robotic arm and the mobile robot. A similar result was also found in scenario L3 with batten light N on and batten light S off, where the luminosities of the markers at M1 or M3 (*i.e.* 76 lx or 79 lx) were about 50 lx brighter than those at M2 or M4 (*i.e.* 26 lx or 27). It should be noted that the minimum luminance of the marker M3 in scenario L4 (*i.e.* 13 lx) was lower than the lowest brightness required for the working area in a construction site (*i.e.* 15 lx) according to the reference [33].

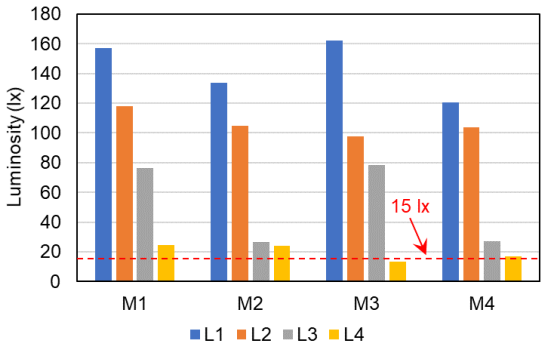

Figure 6. Luminosities on surfaces of fiducial markers at M1, M2, M3 and M4 in different luminance scenarios L1, L2, L3 and L4.

Figure 7 presented the coordinates $(x_{i,j}, y_{i,j})_{cam}$ in the camera coordinate system of the markers and their standard deviations at locations M1, M2, M3 and M4 observed under environmental luminance conditions L1, L2, L3 and L4. As shown in Figure 7(a), after the mobile robot was aligned parallel to MC-1a in scenario L1 (*i.e.* 157 lx), the observed coordinates in camera coordinate system of the marker at M1 were around (0.096 mm, 0.111 mm)$_{cam}$. They were offset to (0.086 mm, 0.162 mm)$_{cam}$ when batten light N was turned off in L2 (*i.e.* 118 lx), or to (0.086, 0.124)$_{cam}$ when batten light S was turned off in L3 (*i.e.* 76 lx). When both lights (*i.e.* batten lights S and N) were turned off in L4 (*i.e.* 25 lx), the observed coordinates of the marker were offset to (0.097 mm, 0.173 mm)$_{cam}$. Thus, it can be identified that the observed coordinates of the markers were shifted from the initial coordinates observed in scenario L1 with the brightest luminance, if the environmental luminance level became lower.

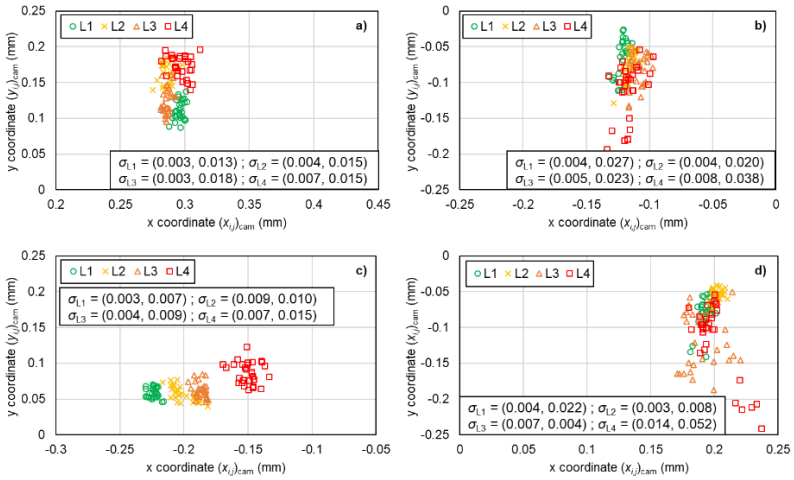

Figure 7. Coordinates of markers at **(a)** M1; **(b)** M2; **(c)** M3 and **(d)** M4 observed in luminance scenarios L1, L2, L3 and L4.

The observation of the coordinates of the markers at M2, M3 and M4 led to a similar conclusion. Specifically, at M2, the observed coordinates of the marker were (0.122 mm, 0.068 mm)$_{cam}$ in L1 (*i.e.* 134 lx) and these coordinates were shifted to (0.117 mm, 0.111 mm)$_{cam}$ when observed in L4 (*i.e.* 24 lx) as shown in Figure 7(b). At M3, the coordinates of the marker at M3 were (0.076 mm, 0.060 mm)$_{cam}$ in L1 (*i.e.* 162 lx) and shifted to (0.151 mm, 0.086 mm)$_{cam}$ when observed in L4 (*i.e.* 13 lx) as shown in Figure 7(c). At M4, the coordinates of the marker were (0.193 mm, 0.079 mm)$_{cam}$ when observed in L1 (*i.e.* 121 lx) and became (0.200 mm, 0.115 mm)$_{cam}$ when observed in L4 (*i.e.* 17 lx) as shown in Figure 7(d). However, the differences in marker coordinates observed under various environmental luminance conditions were found to be insignificant (less than 0.25 mm) compared with the robotic system [29], where differences of 6 mm were reported under comparable luminance environments. This level of variation is well within the accuracy range of the positioning system, as determined to be approximately 2 mm [10], and was also demonstrated in the experiment [7] as acceptable for the robotic construction. In addition, there is a high probability that it may not be necessary to repeat the alignment of the mobile robot or to retarget the component if the observed coordinates in various environmental luminance conditions are all less than 0.5 mm. This is because the condition for repeating alignment of the mobile robot or retargeting the component is that observed coordinate of the marker in the camera coordinate system $(x_{i,j})_{cam}$ or $(y_{i,j})_{cam}$ becomes larger than 0.5 mm, or observed orientation of the marker in camera coordinate system $(r_{zi,j})_{cam}$ becomes larger than 0.25° [7].

Figure 7 also showed the standard deviations (σ) of the coordinates of the markers observed in different environmental luminance conditions. It can be seen that variations in coordinates of the marker observed in each scenario increased as the luminance level decreased. The standard deviations of the coordinates of the marker at M1 observed in L1 were 0.003 mm in x direction and 0.013 in y direction, and these standard deviations were increased to 0.007 mm in x direction and 0.015 mm in y direction when the marker was observed in environmental luminance L4 as shown in Figure 7(a). Similar conclusions were also found in the coordinates of the markers at M2, M3 and M4 (see Figure 7(b), (c) and (d)). This means that the precision in identifying coordinates of the marker became lower when the positioning system was used to observe a marker in a lower lighting environment.

Figure 8 illustrates the observed orientation $(r_{zi,j})_{cam}$ in camera coordinate system of the markers at M1, M2, M3 and M4 and corresponding standard deviations, in environmental luminance L1, L2 L3 and L4. The absolute maximum observed orientations of the markers at M1, M2, M3 and M4 were 0.14°, 0.16°, 0.12°, 0.10° respectively in scenario L1. In L2, the absolute maximum observed orientations of the same markers were comparable to those in L1, with the values of 0.11°, 0.17°, 0.07° and 0.11°. However, in L3, the absolute maximum observed orientations of the markers M1, M2, M3 and M4 increased to 0.22°, 0.24°, 0.21°, 0.09°, respectively. Thus, it can be seen that after proceeding the alignments of the mobile robot and targeting of the component, all the thirty orientational data of each marker observed in environmental luminance L1, L2 and L3 were within 0.25°. It also means that there is no need to realign the mobile robot and targeting the component in environmental luminance L1, L2 and L3, due to the acceptable accuracy (*i.e.* $r_{zi,j} < 0.25°$) in identification of orientation of the marker.

On the other hand, under environmental luminance L4, when both the batten lights were turned off, the absolute values of maximum orientations of the markers M1, M2, M3 and M4 were recorded as 0.26°, 0.28°, 0.38° and 0.28°, respectively. As shown in Figure 8, according to the collected orientations of the markers under environmental luminance L4, about 1/30 or 3% of M1 orientational data, 2/30 or

7% of M2 orientational data, 9/30 or 30% of M3 orientational data, and 3/30 or10% of M4 orientational data exceeded 0.25°. Consequently, the mobile robot alignment and the component targeting phase may be repeated multiple times due to the orientational offsets of the markers when observed under L4 with the lowest environmental luminance. This means, if the observed orientation of marker at M1 or M3 in the camera coordinate system from scenario L4 exceeds 0.25°, the mobile robot may need to rotate about z_m axis to align itself parallel to the installed main component (*i.e.* MC-1a or MC-2a). This additional rotation may increase construction time, as each rotation takes about 30 seconds. Similarly, if the observed orientation of marker at M2 or M4 from L4 exceeds 0.25°, the end-effector of the robotic arm may need to rotate to align the targeting component (*i.e.* CC-3) parallel to the gripper, which takes about 3 seconds. Furthermore, it can be seen that the standard deviations (σ) of the orientations of the markers M1, M2, M3 and M4 observed in different environmental luminance were comparable and all relatively large (approximately 0.05° in average, see Figure 8).

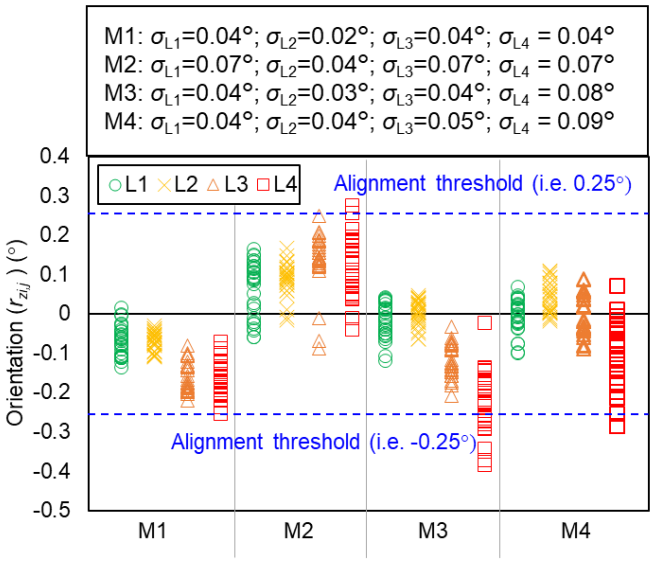

Figure 8. Orientations of markers at a) M1; b) M2; c) M3 and d) M4 observed in luminance scenarios L1, L2, L3 and L4.

The total times of the robotic system to install the components MC-2a and CC-3 were shown in Figure 9 for different environmental luminance scenarios, with the corresponding standard deviations. When one light (*i.e.* batten light S or N) was turned off (*i.e.* environmental luminance L2 or L3, with 106 lx and 52 lx, respectively), the average installation time of thirteen tests was about 170 s, which was increased by 6.3% compared to the average installation time of 161 s in environmental luminance L1 where batten lights N and S are on. In the environment with the lowest luminance L4 where both lights were off, the average installation time was about 25 s (about 13.9%) on average longer in comparison to that in the brightest environment L1 with both lights on. However, the shortest installation times (*i.e.* 117 s, 118 s, and 127 s) in moderate and low light environments L2, L3 and L4 (*i.e.* 106 lx, 52 lx, and 20 lx) seemed to be comparable with that (*i.e.* 140 s) in the environment L1 where both batten lights were on (*i.e.* 144 lx), indicating that the system can still perform reasonably well even in such luminance conditions. In the lowest luminance environment L4, the maximum construction time reached 274 s, which may be resulted from the low accuracy of the positional and orientational data as explained above

(*i.e.* Figure 7 and Figure 8) and therefore more time was required to align the mobile robot parallel to the installed component MC-1a or MC-2a and targeting component MC-2a or CC-3.

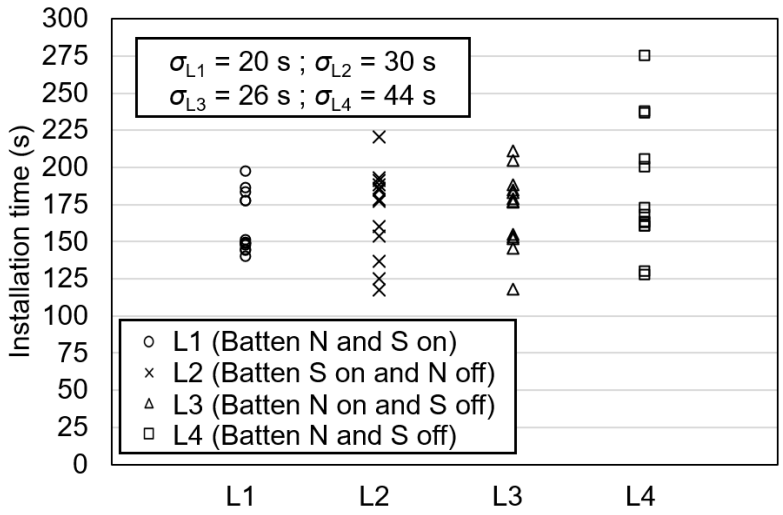

Figure 9. Installation time used for assembly of components MC-2a and CC-3 in different luminance scenarios.

As shown in Figure 9, the standard deviation of the installation time in scenario L1 was 20 s and this increased to 30 s in scenario L2, or 26 s in scenario L3, when the environmental luminance was reduced from 144 lx in L1 to 106 lx in L2, or 52 lx in L3. The standard deviation further increased to 44 s in L4 when environmental luminance further decreased to 20 lx. This means the uncertainly in time became larger in comparison to that in other environments (*i.e.* L1, L2, and L3), because of the need in L4 to complete the same tasks for targeting the components (*i.e.* MC-2a and CC-3) through the markers at M2 and M4 and for aligning the mobile robot parallel to the installed components (*i.e.* MC-1a and MC-2a) through markers at M1 and M3. Again, this may be attributed to the larger differences (*i.e.* less precision) in the positions and orientations of the markers at locations M3 and M4 when they were identified in L4 as shown in Figure 7 and Figure 8. It should be noted, however, that as observed from all scenarios, the environmental luminance as investigated in the present range, did not affect the success of the introduced robotic system. The constructions were all completed even in environmental luminance L4 with the luminance (*i.e.* 13 lx) at M3 and M4 lower than the minimum required luminance (*i.e.* 15 lx) for working area in construction [37].

3.2. Obstacle pattern effects

Figure 10 indicates the success rate of the robotic assembly under different patterns of obstacles on the ground, with thirteen repeating experiments conducted for each obstacle pattern scenario. In scenarios T1 and T2 (see Figure 5b and 5c), where humps C and D were not placed on the ground to interrupt the alignment of the mobile robot, all thirteen tests were completed successfully with the installation of both components MC-2a and CC-3. However, in scenarios T3 and T4, where humps C and D were present, the construction sometimes failed, mainly because one front wheel of the mobile robot rested on hump C or hump D (see the right front wheel in Figure 11a), while the other front wheel still sat on the ground during the installation of the component (see the left front wheel in Figure 11a).

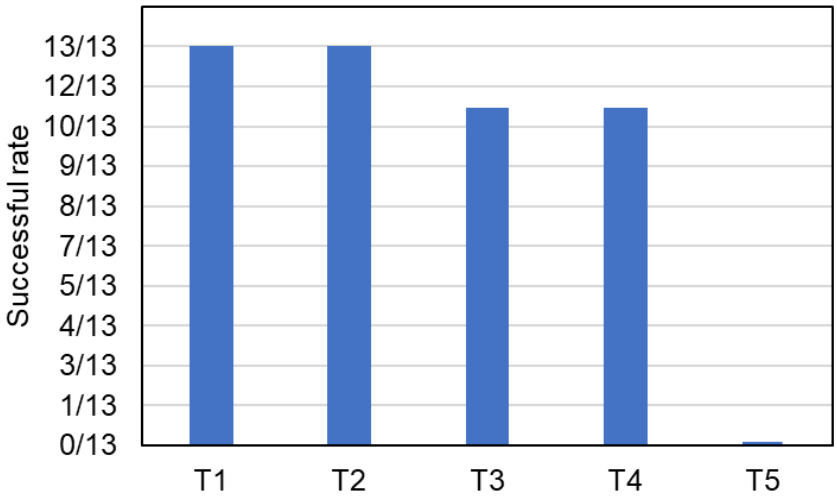

Figure 10. Success rate of installation of components MC-2a and CC-3 in scenarios with different obstacle patterns.

An overall view is shown in Figure 11b for the seventh test in scenario T4 as an example, where the right front wheel of the mobile robot was on the hump D and the left front wheel was on the ground. This caused the mobile robot to tilt, making it impossible for the robotic arm to install the component CC-3 based on the calculated pose for its installation, since the mobile robot and the support of the structure were initially defined to be on the same ground surface. Therefore, only the magnet C-$CC_{3,3}$ of component CC-3 was matched with magnet C-$MC_{2a,3}$ of component MC-2a, and the magnet C-$CC_{3,4}$ of CC-3 was not able to be matched with C-$MC_{2b,3}$ of MC-2b (see the red circle in Figure 11b). Consequently, this resulted in a success rate of 85% for both T3 and T4 scenarios (see Figure 10).

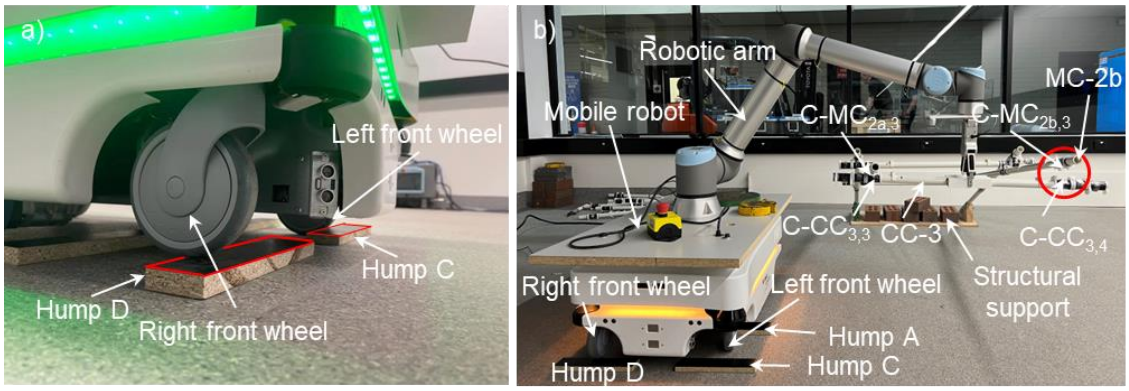

Figure 11. Failure mode in scenarios T3 and T4 due to misalignment of mobile robot to component MC-2a: **(a)** disturbance of the humps and **(b)** an overview of the seventh test.

In scenario T5 the spacing between humps A, B and humps C, D was narrow (*i.e.* 100 mm) in comparison to that of 150 mm in scenarios T3 and T4. This constrained the movement of both front wheels (with a diameter of 125 mm) of the mobile robot as shown in Figure 12. As a result, it did not allow the alignment to proceed as programmed; and the installation of component CC-3 did not proceed in all the tests in this scenario (see Figure 10).

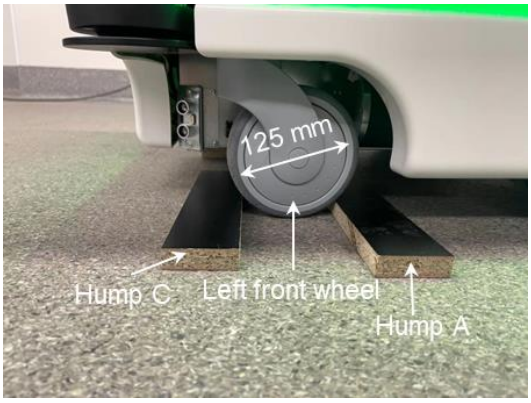

Figure 12. Failure mode of constrained front wheels due to a narrow clearance between hump C and hump A in scenario T5.

Even for the tests in scenarios T3 and T4 where the installations of MC-2a and CC-3 were successful, as the mobile robot passed over the humps A and/or B, its orientation was altered in some cases due to the disturbances caused by these obstacles. Such changes in the orientation (*i.e.* Δr_{zm}) are shown in Figure 13, for all tests in scenarios T1, T2, T3 and T4. On average, the orientation of the mobile robot was changed by 0.20° when passing the humps A and B in scenario T1 and by 0.21° in scenario T3. On the other hand, when the mobile robot passed the hump A only, its orientation was changed by 0.49° in scenario T2 and by 0.44° in scenario T4. As illustrated in Figure 13, the maximum orientational changes of the mobile robot when passing hump A only in T2 and T4 scenarios (*i.e.* 0.95°, 1.00°) were approximately double of that of the mobile robot when passing humps A and B in T1 and T3, which were 0.52° and 0.58°, respectively. After passing the humps A and B, the mobile robot needed to be aligned parallel to the installed component MC-2a if the difference between the orientation of the robot and the installed component MC-2a was greater than 0.25°, and more construction time would be required accordingly.

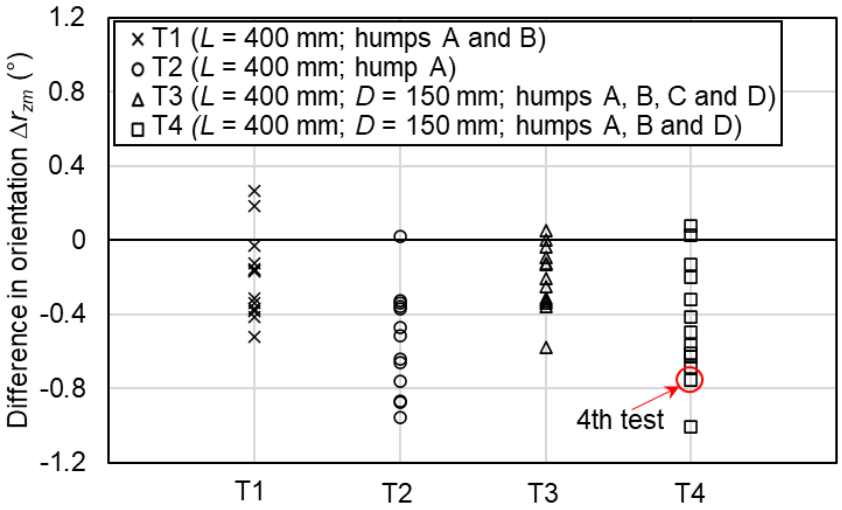

Figure 13. Difference in orientation (Δr_{zm}) of mobile robot before and after passing humps A and B.

Figure 14 illustrates the construction time and its standard deviation in the scenarios of different obstacle patterns if the installation was completed (*i.e.* T1, T2, T3 and T4). As shown in Figure 14, the average construction time in scenario T4 was about 259 s. This was much longer than the average

construction time in T1, T2, and T3 (*i.e.* 169 s, 161 s, and 162 s, respectively). The minimum installation times in different scenarios seemed to be still comparable, where it was 148 s in T1, 146 s in T2, 116 s in T3 and 158 s in T4. However, the maximum installation time of T4 reached 531 s which was significantly different from other scenarios (*i.e.* 206 s in T1; 205 s in T2 and 203 s in T3). It can be further found from the fourth test in T4 scenario that took the longest construction time of 531 s (see the red circle in Figure 14), the orientation of the mobile robot changed by 0.75° (see the red circle in Figure 13) mainly due to the asymmetry of the humps (see Figure 5(e)). This required the mobile robot to be rotated to align itself parallel to the installed component MC-2a before targeting the component CC-3 during the installation of CC-3. However, during this alignment process, humps C and D interrupted the alignment of the mobile robot by blocking the movement of its front wheels. Therefore, the mobile robot had to spend more time repeating the alignment process to ensure that it was parallel to the installed main component MC-2a.

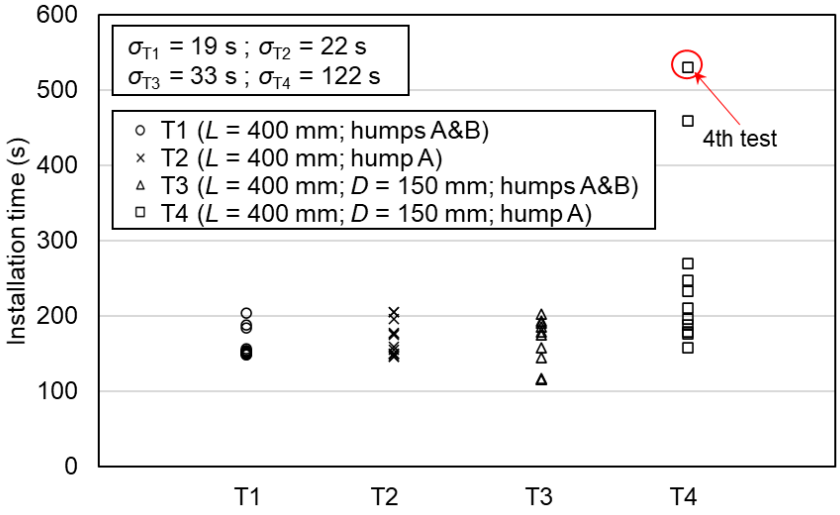

Figure 14. Installation time used for assembly of components MC-2a and CC-3 in different scenarios.

As shown in Figure 14, the standard deviations of the construction time in scenarios T1, T2, and T3 were 19 s, 22 s, and 33 s, respectively. It significantly increased to 122 s for scenario T4. This means that the variation of the construction times (and also the uncertainty) increased in scenario T4 with more humps and asymmetric obstacle pattern.

4. Conclusion

Effects of luminance and obstacle pattern on the accuracy of the positioning system, completion time and successful completion of the robotic structural assembly were studied through physical experiments in this study. Also, the construction time and success rate of the robotic system to complete the installations of selected structural components were evaluated. The following conclusions were obtained based on the results of this investigation:

1) The accuracy of the positions and orientation of the fiducial marker (AprilTag) at different locations, was found to be affected by the environmental luminance levels. The coordinates and orientation of the markers in the camera coordinate system observed in different environmental luminance were generally within the accuracy range of the positioning system. However, in a dark

lighting condition with less than 15 lx, a portion of collected orientational data exceeded the accuracy range of the positioning system. This indicated that the mobile robot could need to rotate multiple times to align itself parallel to the installed component in such lighting conditions.

2) The effectiveness, as measured by construction time, was found to be affected by luminance levels, particularly with regards to the alignment of the mobile robot parallel to the installed component and the alignment of the gripper parallel to the installing component. Such inaccurate marker orientations in the lighting condition of 13 lx caused the increase in the construction time and its standard deviation increased as well, and thus resulting in longer and more uncertain construction times. Nevertheless, with this robotic system, the construction can be completed in all luminance conditions, even when the luminance was reduced to the lowest required luminance of 15 lx for the working area in a construction site.

3) Obstacle disturbance in the construction process led to an increase in construction time, particularly in aligning the mobile robot, and a decrease in success rate. When the mobile robot passed over a symmetric pattern, the change in orientation of the mobile robot were less than the realignment threshold (less than 25°). However, in the case of an asymmetric pattern, the change in orientation was greater than the threshold and thus could lead to a need to rotate the mobile robot, and consequently more construction time. The standard deviation of the construction time in T4 was also relatively greater than that in other scenarios, indicating an increased uncertainty in the construction time when there were more humps and asymmetric obstacle patterns in T4.

4) In scenario T5, where the spacing between the humps A, B and humps C, D was reduced from 150 mm to 100 mm (in comparison to the diameter of 125 mm of the front wheel), both front wheels of the mobile robot were constrained within the humps. This prevented the alignment of the mobile robot from proceeding as programmed, and as a result, the installation could not be completed in all tests in this scenario.

The findings from this study provide quantifications and insights into the impact of important environmental factors on robotic construction, thereby helping to ensure its functionality and effectiveness under realistic environmental conditions. Further experiments may be expected to investigate and understand the performance of robotic systems for construction under realistic environmental conditions such as dust, fume or fog, and wind or even rain. Furthermore, although AprilTag markers offer high positional accuracy, they may be covered by dust or damaged. Therefore, a more robust positioning algorithm can be valuable. For instance, using the AprilTag-derived coordinates to train a deep learning model may improve accuracy of positioning system on actual construction sites.

Acknowledgments

The authors are grateful for support from the Australian Research Council through LP180101080. Thanks are also given to Pascal Mater and Zoltan Csaki at Monash Civil Engineering for their technical assistance with electrical configuration and component manufacturing.

Authors' contribution

Cheav Por Chea: Conceptualization, Methodology, Software, Validation, Formal analysis, Investigation, Data curation, Writing – original Draft Preparation, Visualization. Yu Bai: Conceptualization, Methodology, Investigation, Resources, Supervision, Project Administration, Funding Acquisition. Yihai Fang: Writing – Review

and Editing, Supervision. Elahe Abdi: Writing – Review and Editing, Supervision. All authors have read and agreed to the published version of the manuscript.

Conflicts of interests

The authors declare no conflict of interest.

References

[1] Yu N, Lee Y, Han S, Lee Y, Lee H. Development of the curtain wall installation robot: performance and efficiency tests at a construction site. *Auton. Rob.* 2007, 22:281–291.

[2] Kumagai I, Morisawa M, Sakaguchi T, Nakaoka SI, Kaneko K, *et al*. Toward industrialization of humanoid robots: autonomous plasterboard installation to improve safety and efficiency. *IEEE Robot Autom Mag.* 2019, 14;26(4):20–29.

[3] Lee S, Nam H, Lee Y, Park J. A new type of bolting robot for steel-frame structure constructions. In *Proceedings of the 2008 International Conference on Control, Automation and Systems*, Seoul, Republic of Korea, October 14, 2008, pp. 2256–2260.

[4] Chu B, Jung K, Chu Y, Hong D, Lim MT, *et al*. Robotic automation system for steel beam assembly in building construction. In *Proceedings of the 2009 4th International Conference on Autonomous Robots and Agents*, Wellington, New Zealand, Febuary 10, 2009, pp. 38–43.

[5] Pritschow G, Dalacker M, Kurz J. Configurable control system of a mobile robot for on-site construction of masonry. In *Proceedings of the 10th International Symposium on Robotics and Automation in Construction*, Houston, USA, May 24, 1993, pp. 85–92.

[6] Chea CP, Bai Y, Pan X, Arashpour M, Xie Y. An integrated review of automation and robotic technologies for structural prefabrication and construction. *Transp. Saf. Environ.* 2020, 2(2):81–96.

[7] Chea CP, Bai Y, Zhou Z. Design and development of robotic collaborative system for automated construction of reciprocal frame structures. *Comput.-Aided Civ. Infrastruct. Eng.* 2024, 39(10):1550–1569.

[8] Chea CP, Bai Y, Fang Y, Zhang Y. Geometric forming and mechanical performance of reciprocal frame structures assembled using fibre reinforced composites. *Eng. Struct.* 2022, 250:113420.

[9] Bock T, Linner T. *Robot oriented design*. Cambridge: Cambridge university press, 2015.

[10] Chea CP, Bai Y, Fang Y. Positional inaccuracy investigation and innovative connection solution for robotic construction of load carrying structures. *J. of Infrastruct. Intell. Resil.* 2025, 4(2):100141.

[11] Vargas J, Alsweiss S, Toker O, Razdan R, Santos J. An overview of autonomous vehicles sensors and their vulnerability to weather conditions. *Sensors* 2021, 21(16):5397.

[12] Zang S, Ding M, Smith D, Tyler P, Rakotoarivelo T, *et al*. The impact of adverse weather conditions on autonomous vehicles: how rain, snow, fog, and hail affect the performance of a self-driving car. *IEEE Veh. Technol. Mag.* 2019, 14(2):103–111.

[13] Chaudhary S, Wuttisittikulkij L, Saadi M, Sharma A, Al Otaibi S, *et al*. Coherent detection-based photonic radar for autonomous vehicles under diverse weather conditions. *PLoS One* 2021, 16(11):e0259438.

[14] Laible S, Khan YN, Bohlmann K, Zell A. 3D lidar-and camera-based terrain classification under different lighting conditions. In *Proceedings of the 22nd Autonomous Mobile Systems*, Stuttgart, Germany, September 26–28, pp. 21–29.

[15] Choudhary S, Sharma R. Perceived dominating colors optimization for camouflage texture generation & its effect evaluation. In *Proceedings of the 4th International Conference on Recent Trends in Computer Science and Technology*, Jamshedpur, India, Febuary 11, 2022, pp. 334–339.
[16] Lee G, Kim HH, Lee CJ, Ham SI, Yun SH, *et al*. A laser-technology-based lifting-path tracking system for a robotic tower crane. *Autom. Constr.* 2009, 18(7):865–874.
[17] Win TM. Robotic Tower Crane Modelling Control (RTCMC), Doctoral Thesis, UNSW, 2017.
[18] Yamauchi B. All-weather perception for man-portable robots using ultra-wideband radar. In *Proceedings of the 2010 IEEE International Conference on Robotics and Automation*, Anchorage, USA, May 3, 2010, pp. 3610–3615.
[19] Chen W, Zhang F, Gu T, Zhou K, Huo Z, *et al*. Constructing floor plan through smoke using ultra wideband radar. In *Proceedings of the ACM on Interactive, Mobile, Wearable and Ubiquitous Technologies*, New York, USA, December 30, 2021, 5(4):1–29.
[20] Vähä P, Heikkilä T, Kilpeläinen P, Järviluoma M, Gambao E. Extending automation of building construction—Survey on potential sensor technologies and robotic applications. *Autom. Constr.* 2013, 36:168–178.
[21] Hong S, Shyam P, Bangunharcana A, Shin H. Robotic mapping approach under illumination-variant environments at planetary construction sites. *Remote Sens.* 2022, 14(4):1027.
[22] Chen X, Huang H, Liu Y, Li J, Liu M. Robot for automatic waste sorting on construction sites. *Autom. Constr.* 2022, 141:104387.
[23] Jian X, Li J, Chen X, Chen J, Wen Y, *et al*. The robot maintenance method for fitting bolt in high-altitude settlement environment. In *Proceedings of the 2021 China Automation Congress*, Beijing, China, October 22, 2021, pp. 8101–8106.
[24] Hsu QC, Ngo NV, Ni RH. Development of a faster classification system for metal parts using machine vision under different lighting environments. *Int. J. Adv. Manuf. Technol.* 2019, 100:3219–3235.
[25] Mneymneh BE, Abbas M, Khoury H. Vision-based framework for intelligent monitoring of hardhat wearing on construction sites. *J. Comput. Civ. Eng.* 2019, 33(2):04018066.
[26] Li D, Xie Q, Gong X, Yu Z, Xu J, *et al*. Automatic defect detection of metro tunnel surfaces using a vision-based inspection system. *Adv. Eng. Inform.* 2021, 47:101206.
[27] Wijayathunga L, Rassau A, Chai D. Challenges and solutions for autonomous ground robot scene understanding and navigation in unstructured outdoor environments: a review. *Appl. Sci.* 2023, 13(17):9877.
[28] Delgado JM, Oyedele L. Robotics in construction: a critical review of the reinforcement learning and imitation learning paradigms. *Adv. Eng. Inform.* 2022, 54:101787.
[29] Chen L, Hussain A, Liu Y, Tan J, Li Y, *et al*. A novel multi-sensor nonlinear tightly-coupled framework for composite robot localization and mapping. *Sensors* 2024, 24(22):7381.
[30] Apolinarska AA, Pacher M, Li H, Cote N, Pastrana R, *et al*. Robotic assembly of timber joints using reinforcement learning. *Autom. Constr.* 2021, 125:103569.
[31] Zhou Z, Abdi E, Chea CP, Bai Y. Global path planning for autonomous construction vehicles in building construction: a comparative study with a focus on vehicle kinematic characteristics. *J. Build. Eng.* 2024, 93:109837.
[32] Lenain R, Thuilot B, Hach O, Martinet P. High-speed mobile robot control in off-road conditions: a multi-model based adaptive approach. In *Proceedings of the 2011 IEEE International Conference on Robotics and Automation*, Shanghai, China, May 9, 2011, pp. 6143–6149.

[33] Czapla T, Fice M, Niestrój R. Experimental identification of wheel-surface model parameters: various terrain conditions. *Sci. Rep.* 2022, 12(1):16015.

[34] Mastalli C, Focchi M, Havoutis I, Radulescu A, Calinon , *et al*. Trajectory and foothold optimization using low-dimensional models for rough terrain locomotion. In *Proceedings of the 2017 IEEE International Conference on Robotics and Automation*, Singapore, May 29, 2017, pp. 1096–1103.

[35] Yokogawa. 510 01 and 510 02 Digital Illuminance Meters. Available at: http://www.transcat.com/media/pdf/510_digitalilluminancemeters.pdf (accessed on 21 February 2023).

[36] Mobile Industrial Robot. Specifications for MiR 100. Available: https://www.mobile-industrial-robots.com/solutions/robots/mir100/ (accessed on 30 July 2021).

[37] Chudley R, Greeno R. *Building construction handbook*. Abingdon: Routledge, 2006, pp. 90.